INTERNATIONAL DESIGN CONFERENCE – DESIGN 2024
https://doi.org/10.1017/pds.2024.174

Additively manufactured 3D micro scarf adhesive joints

Michael Ascher ✉ and Ralf Späth

Bundeswehr University Munich, Germany

✉ michael.ascher@unibw.de

Abstract

Hybrid manufacturing enables to overcome additive manufacturing (AM) constraints regarding the maximum feasible part dimension and/or complexity through part separation and subsequent adhesive joining of AM sub-parts. To ensure structural integrity of the joint at a minimum use of substrate volume, the AM inherent freedom of design can be exploited by realizing 3D micro scarf adhesive joints. The performance of this novel adhesive joint design was assessed by conducting optical measurements and static tensile tests using samples fabricated by laser-based powder bed fusion of metals (PBF-LB/M).

Keywords: additive manufacturing, lightweight design, hybrid manufacturing, powder bed fusion, scarf adhesive joint

1. Introduction

Additive Manufacturing (AM) processes enable to overcome various limitations with geometry realization compared to traditional manufacturing methods. This can be exploited by adding more functions to a single component (Yang and Zhao, 2015) or by realizing functionally graded materials (Panesar et al., 2018) or complex designs obtained from numerical topology optimization (Yang et al., 2017). In case of the laser-based powder bed fusion process for metals (PBF-LB/M), manufacturing costs rise with increased part complexity. This is due to increased manufacturing time and a higher expense on support structure and post-processing (Reichwein and Kirchner, 2021). Additional design restrictions arise due to the confined building space of the manufacturing machines and requirements regarding the removal of powder residues from the PBF-LB/M parts after the build job is finished. They are limiting the feasible maximum part dimensions and/or complexity and therefore the usability of PBF-LB/M processes for various applications. Hybrid manufacturing, which means part separation and subsequent joining of AM sub-parts, can be an effective way of overcoming these limitations while reducing manufacturing cost (Reichwein et al., 2022).

Adhesive bonding provides great potential for joining of AM sub-parts for not imposing restrictions on the joining surfaces geometry or the substrates material. To ensure structural integrity of the joined part, it is necessary to adapt the design of the joint to the external load (Ebnesajjad and Landrock, 2015). This means that a sufficiently large adhesive surface area is provided and that the adhesive is primarily loaded in shear and not tension (Banea and Da Silva, 2009). In general, adhesive joint designs can be distinguished between lap joints (LJ) and butt joints (BJ). In LJs two overlapping substrates are joined by bonding larges surfaces of each substrate resulting in a large adhesive surface area. For realization, the substrates must offer the corresponding geometrical requirements and there is additional weight introduced by the overlapping substrates. The BJ is a less complex joint design as the two substrates are simply joined end to end at their front surfaces. As the adhesive surface area is comparably small and the adhesive is primarily stressed in tension (for tensile loading), this design is rarely used for applications with high strength requirements. One way to improve the strength characteristics of a BJ is

to cut opposing tapered ends on each substrate which are then joined. In the following this will be referred to as the one-dimensional scarf adhesive joint (1D SAJ, Figure 1, left). The larger the taper angle (scarf angle α), the larger the adhesive surface area gets and the more the adhesive stress state is shifted from tension to shear. Both effects are increasing the bearable load of the joint. A disadvantage of 1D SAJs is the additional substrate volume required in the tapering direction. This volume is proportional to the scarf angle α, and it is quantified by it´s mounting height h. In order to reduce the mounting height, it is possible to taper the ends of the substrates in two directions (Figure 1, right) resulting in a wedge profile (double scarf adhesive joint (Gacoin et al., 2009) or 2D SAJ). For each additional wedge introduced to the front surface of a substrate, the mounting height, as well as the base length a of the wedge, is reduced proportionally.

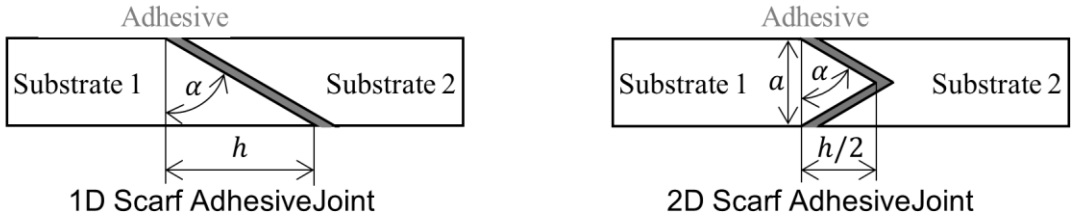

Figure 1. Characteristic appearance and dimensions of1D (left) and 2D (right) SAJs

As in many applications AM components feature complex and thin-walled geometrical features, the applicability of the AM design approach of part separation and subsequent adhesive bonding of AM sub-parts is either restricted due to an insufficient adhesive surface area (and thus insufficient load-bearing capacity) or an insufficient substrate volume for the realization of scarf adhesive joints. Therefore, the primary objective of this research is to improve to the applicability of hybrid manufacturing by assessing the feasibility of tapering an adhesive scarf joint in multiple planes (3D micro scarf adhesive joint or 3D µSAJ) to maximize the bearable load to mounting height ratio. Since the triangular pyramid offers a superior ratio of lateral surface (adhesive surface area) to base surface area of $r_{tri} = 2$ ($h = 0.5$ mm) compared to the corresponding ratios of the square pyramid ($r_{sq} = 1.75$), the pentagonal pyramid ($r_{pent} = 1.49$) or the cone ($r_{cone} = 1.68$) having an identical mounting height. Therefore, triangular pyramid geometry samples featuring different base triangle side lengths and scarf angles were manufactured utilizing the PBF-LB/M process with the aluminium alloy AlSi10Mg (PBF-LB/M/AlSi10Mg). The geometry samples represent the positive pyramids that are applied to the front surface of the first substrate, as well as the corresponding negative pyramids that are imprinted into the front surface of the second substrate. By optical measurement of the geometry samples using a 3D laser scanning microscope, the joints performance was quantified considering manufacturing inaccuracies and measures for improving the accuracy of fit were derived. Subsequently PBF-LB/M/AlSi10Mg 3D µSAJ tensile samples were manufactured and subjected to static tensile tests. The resulting bonding strength is compared to the bonding strength of corresponding PBF-LB/M/AlSi10Mg 1D SAJs and PBF-LB/M/AlSi10Mg adhesive butt joints (ABJs).

2. Materials and methods

2.1. Optical measurement of triangular pyramid geometry samples

Depending on the PBF-LB/M process variables, the minimum manufacturable geometrical feature size is limited (Diegel et al., 2019). Therefore, it is not possible to represent the sharp peaks of positive and negative pyramids from the computer-aided design (CAD) data in the PBF-LB/M parts. It can be expected that the more acute the scarf angle becomes, the more actual mounting height and adhesive surface area is lost. The extent of this manufacturing inaccuracy is expected to differ between positive and negative pyramids, which will have a negative impact on the accuracy of fit. To derive measures for improving the accuracy of fit and to quantify the performance of the joint as a function of the scarf angle, positive and negative PBF-LB/M/AlSi10Mg pyramids with varying scarf angle and identical base triangle side length were manufactured and optically measured using a 3D laser scanning microscope.

As the minimum base triangle side length is limited for the same reason, positive and negative PBF-LB/M/AlSi10Mg pyramids with varying base triangle side length and identical scarf angle were subjected to the same procedure. With the results obtained, measures for improving the accuracy of fit were derived and the performance of the joint was quantified as a function of the base triangle side length. The nominal dimensions of the pyramid geometry samples subjected to optical measurement are represented in Table 1.

Table 1. Nominal dimensions of PBF-LB/M/AlSi10Mg triangular pyramid geometry samples

Sample	Nominal Side Length a_{nom} in mm	Nominal Scarf Angle α_{nom} in °	Nominal Mounting Height h_{nom} in mm
Equilateral Base Triangle Side Length Variation #1 Positive: 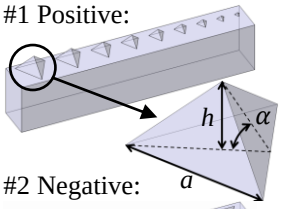 #2 Negative: 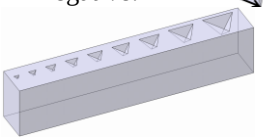	3.00	60	1.50
	2.50		1.25
	2.00		1.00
	1.75		0.875
	1.50		0.75
	1.25		0.625
	1.00		0.50
	0.75		0.375
	0.50		0.25
Scarf Angle Variation #3 Positive: 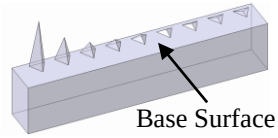 #4 Negative: 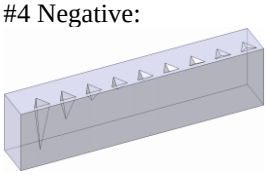	1.5	85	4.95
		80	2.46
		70	1.19
		60	0.75
		50	0.52
		40	0.36
		30	0.25
		20	0.16
		10	0.08

The samples were manufactured standing upright using a *Trumpf TruPrint 1000* manufacturing machine and AlSi10Mg powder with a particle size of 20 µm to 63 µm. The respective machine parameters and an exemplary scan pattern of a positive pyramid geometry sample is depicted in Table 2.

Table 2. Machine parameters used for manufacturing the PBF-LB/M/AlSi10Mg samples

Parameter	Unit	Value	Exemplary Scan Pattern
Scanning Speed	mm/s	1815	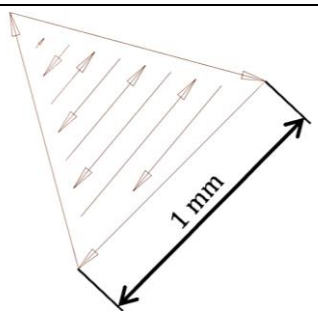
Laser Power	W	175	
Layer Thickness	µm	20	
Laser Spot Size	µm	55	
Laser Beam Compensation	µm	40	
Hatch Spacing	µm	90	
Rotation Angle of Scan Pattern	°	45	

To determine the actual dimensions of the pyramids according to Table 1, the printed samples were placed standing upright on the machine bed of 3D laser scanning microscope (*Keyence VK-X 3000*). The height profile was captured with a measuring resolution of *1* µm. From the height profile, the actual mounting height h of the pyramid is established by measuring the distance from the highest/lowest point of the positive/negative pyramid to a reference plane, which is defined by the topography of the pyramid geometry samples base surface (see Table 1) using the method of ordinary least squares (Figure 2, left). The side length a of the pyramids base triangle is determined by first generating three auxiliary lines through a height-based edge detection at the transition from the base into the lateral surfaces of the pyramid. Next, the intersection points of the auxiliary lines are generated, and the distances of the intersection points are measured. The actual side length a results as the average of the three measured distances (Figure 2, right).

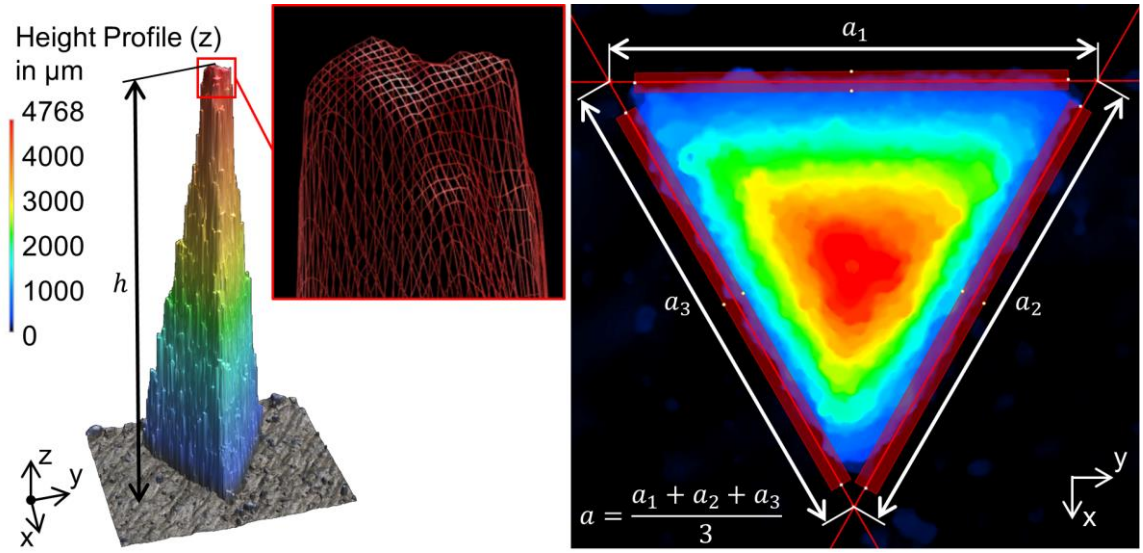

Figure 2. Height Profile of a positive triangular pyramid (a_{nom}=1.5 mm; α_{nom}=85° and h_{nom}=4.95 mm) and evaluation of the actual mounting height h (left) and actual base triangle side length a (right)

2.2. Static tensile tests

To determine the bonding strength of 3D µSAJs and to compare the results with ABJs and 1D SAJs, static tensile tests based on EN 15870:2009-08 (EN, 2009) were carried out. The nominal geometry and quantity of tensile samples tested is listed in Table 3.

Table 3. Nominal geometry and quantity of ABJ, 1D SAJ and 3D µSAJ tensile samples

Adhesive Butt Joint (ABJ) (8x)	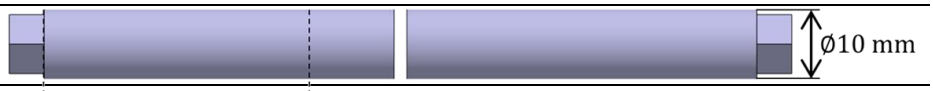
1D Scarf Adhesive Joint (1D SAJ) $\alpha_{nom,1}$ = 80° (5x) $\alpha_{nom,2}$ = 85° (6x)	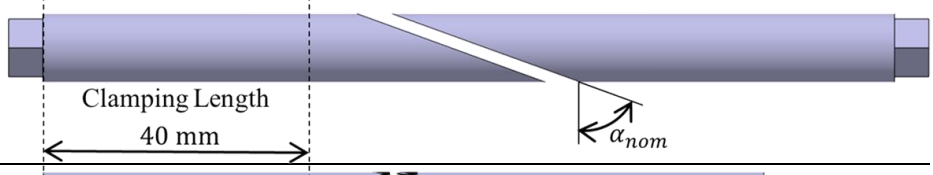
3D Micro Scarf Adhesive Joint (3D µSAJ) a_{nom} = 1.5 mm $\alpha_{nom,1}$ = 80° (8x) $\alpha_{nom,2}$ = 85° (7x)	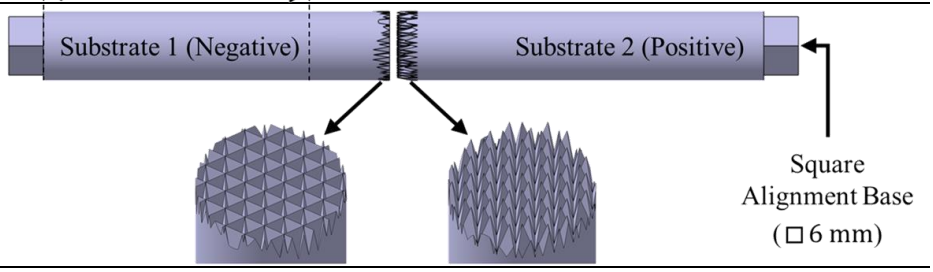

The substrates were manufactured standing upright (square alignment base attached to the build plate) using the same manufacturing machine, machine parameters and AlSi10Mg powder as for the pyramid geometry samples described in section 2.1. After finishing the build job, the substrates were de-powdered and support structures surrounding the square alignment base were removed mechanically. Then the substrates were cleaned in an ultrasonic bath with isopropyl, dried and placed in a 90° prism for concentrical alignment. For radial alignment the square alignment base of the substrates was inserted in corresponding bearing blocks which feature a 90° angle that rests on the prism. One of the bearing blocks is fixed to the prism while the other one can be moved longitudinally by actuating a micrometer screw. To adjust the adhesive gap height, the substrates were merged until the joining surfaces were in contact. Then the micrometer screw was turned back until the nominal adhesive gap height of 0.2 mm was reached (the longitudinal displacement depends on the scarf angle). The corresponding measure of the micrometer screw was noted, and the substrates were removed from the prism in order to apply a two-component epoxy-based structural adhesive (*3M Scotch-Weld DP490*) to the joining surfaces using a scraper. Now the substrates were placed back in the prism and merged by setting the previously noted measure on the micrometer screw. For curing the adhesive, the aligned tensile samples were stored in the oven at 80 °C for one hour and then conditioned to standard climate (23 °C/50%).
The static tensile tests were carried out using an *Instron 8801* servo hydraulic testing machine equipped with a 50 kN force transducer (*Instron MTM 1433*) and wedge grips clamping the tensile samples at a clamping length of 40 mm. To cause the tensile samples to fail within a test time of (60 ± 20) s (EN, 2009) they were loaded at a constant test speed of 0.018 mm/min. Failure applies when the force signal (recorded at a measuring rate of 50 Hz) falls below the maximum measured value. The tests were terminated when the force signal dropped to 60% of maximum measured value.
The bonding strength σ_{Bond} was evaluated by relating the maximum force measured F_{max} to the reference cross section of the tensile samples A_{Ref} according to equation 1.

$$\sigma_{Bond} = F_{max}/A_{Ref} = F_{max}/(r^2\pi) = F_{max}/((5\text{ mm})^2\pi) = F_{max}/78.5\text{ mm}^2 \quad (1)$$

3. Results and discussion

3.1. Optical measurement of triangular pyramid geometry samples

To maximize the bonding strength to mounting height ratio of 3D µSAJs it is necessary to minimize the tensile stress σ acting in the adhesive layer at a minimum base triangle surface area A_{Base} and a minimum nominal mounting height h_{nom}. Therefore, the bonding performance of two joined pyramids can be assessed by evaluating the normalized key performance indicator KPI (Equation 2).

$$KPI = 1/(\sigma^2 * h_{nom} * {A_{Base}}^2 * KPI_{max}) = 1/(\sigma^2 * h_{nom} * \left(0.25 * {a_{nom}}^2 * \sqrt{3}\right)^2 * KPI_{max}) \quad (2)$$

KPI_{max} is the maximum key performance indicator found for merging positive and negative pyramids with identical nominal values on sample #1/#2 respectively #3/#4. The tensile stress σ acting in the adhesive is calculated according to equation 3, where F_x is an arbitrarily selectable tensile load acting on the joint.

$$\sigma = F_x * cos(min(\alpha_+, \alpha_-))/A_{Adh} \quad (3)$$

For the following evaluation $F_x = 1$ kN applies. α_+/α_- are the actual scarf angles applying to positive/negative pyramids with identical nominal values They are derived from the actual mounting height h and actual base triangle side length a according to equation 4.

$$\alpha_{+,-} = arctan((6 * h_{+,-})/(\sqrt{3} * a_{+,-})) \quad (4)$$

A_{Adh} represent the actual adhesive surface area (actual lateral surface area) applying to the smaller positive or negative pyramid with identical nominal values. A_{Adh} is calculated according to equation 5, where a_+/a_- and h_+/h_- depict the actual side lengths and mounting heights of the positive and negative pyramids.

$$A_{Adh} = (3/2) * min(a_+, a_-) * \sqrt{(1/12) * min(a_+, a_-)^2 + min(h_+, h_-)^2} \quad (5)$$

The results obtained for measuring the actual base triangle side length a_+/a_- and mounting height h_+/h_- of positive/negative pyramid geometry samples with varying nominal base triangle side length a_{nom} (Table 1, Samples #1 and #2) are depicted in Figure 3.

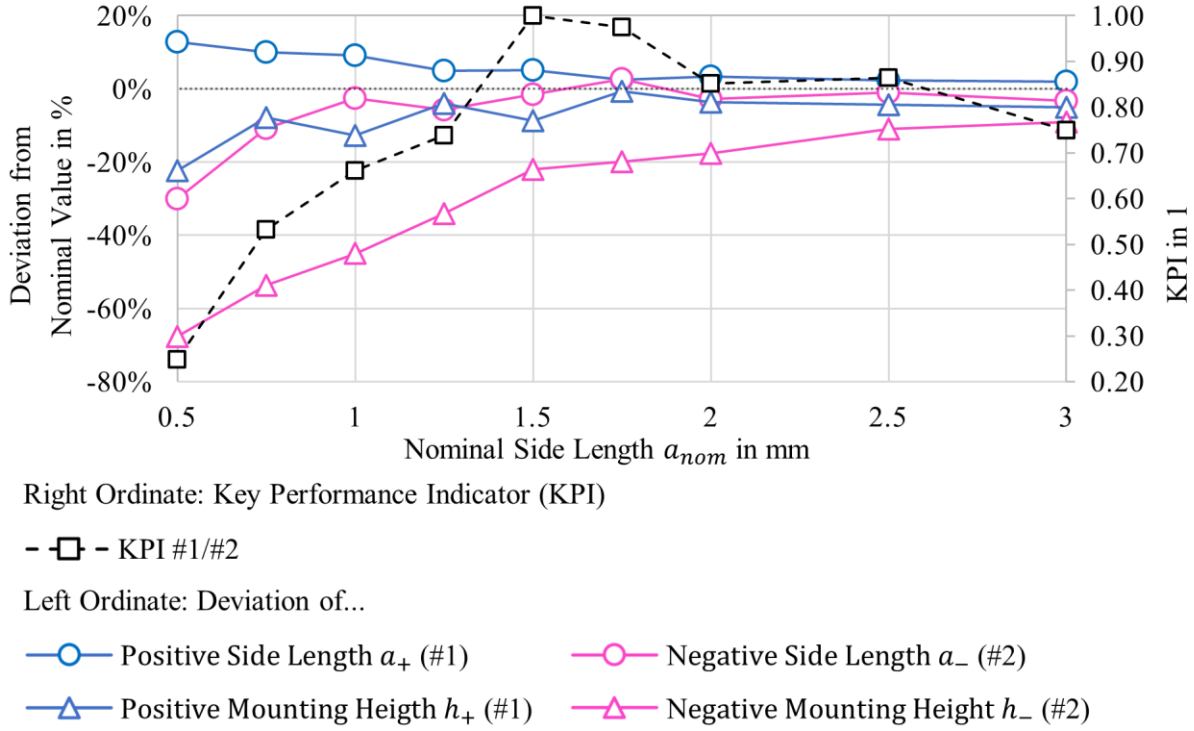

Figure 3. Deviation of the actual base triangle side length a and mounting height h from the respective nominal values and normalized KPI derived from optical measurement of positive (#1) and negative (#2) pyramids with varying nominal base triangle side length a_{nom}

The side lengths of all positive pyramids a_+ exceed and all the negative equivalents a_- (except for $a_{nom} = 1.75$ mm) stay below their respective nominal values. The extend to which the actual values deviate from the nominal values decreases with increasing nominal side length a_{nom}. To improve the accuracy of fit, a reduced (compensated) nominal side length $a_{nom,red}$ for positive pyramids according to equation 6 can be used.

$$a_{nom,red} = a_{nom} * (1 + f_{comp,a}) \tag{6}$$

$$\text{using } f_{comp,a} = \left(0.088 * \frac{a_{nom}{}^3}{\text{mm}^3} - 0.58 * \frac{a_{nom}{}^2}{\text{mm}^2} + 1.2 * \frac{a_{nom}}{mm} - 0.89\right) \text{ for } 0.5 \text{ mm} \leq a_{nom} \leq 3 \text{ mm}$$

The 3rd degree polynomial compensation function $f_{comp,a}$ was calculated using the method of ordinary least squares. The ordinate of the underlying data set results by subtracting the deviation of the positive pyramids side length from the deviation of the negative pyramids side length.
Upon comparing the actual mounting height h_+/h_- of positive/negative pyramids with the respective nominal mounting height h_{nom} it becomes evident that all the actual values stay below their respective nominal values with the deviation increasing for smaller nominal side lengths. As the loss in mounting height of negative pyramids exceeds the loss in mounting height of positive pyramids, the accuracy of fit can be improved by using an increased nominal mounting height $h_{nom,inc}$ for negative pyramids according to equation 7.

$$h_{nom,inc1} = h_{nom} * \left(1 + f_{comp,h1}\right) \tag{7}$$

$$\text{using } f_{comp,h1} = \left(0.061 * \frac{h_{nom}{}^2}{\text{mm}^2} - 0.39 * \frac{h_{nom}}{mm} + 0.66\right)$$

$$\text{for } 0.5 \text{ mm} \leq a_{nom} \leq 3 \text{ mm and } \alpha_{nom} = 60°$$

The 2nd degree polynomial compensation function $f_{comp,h1}$ was determined analogously to the procedure explained in the previous paragraph, only this time the deviation of the actual pyramid's mounting height from the nominal mounting height was used.
Looking at the course of the KPI as a function of the nominal side length a_{nom}, a pronounced maximum occurs at a nominal side length of 1.5 mm. This seems contradictory at first, since theoretically the KPI should continue to increase with the nominal side length a_{nom} decreasing. However, since for nominal side lengths less than 1.5 mm both the actual mounting height and side length of the pyramids are significantly reduced compared to the corresponding nominal value, the advantage of a lower nominal mounting height is outweighed by the loss in actual adhesive surface area. This behaviour is caused by PBF-LB/M/AlSi10Mg limitations regarding the manufacturability of small geometrical features and eventually means that 1.5 mm is the ideal nominal base triangle side length of triangular pyramids for implementing 3D µSAJs using the PBF-LB/M/AlSi10Mg process.
Figure 4 depicts the deviation of the actual mounting height h_+/h_- of positive/negative pyramids from the respective nominal values as well as the corresponding KPI´s for varying nominal scarf angles.

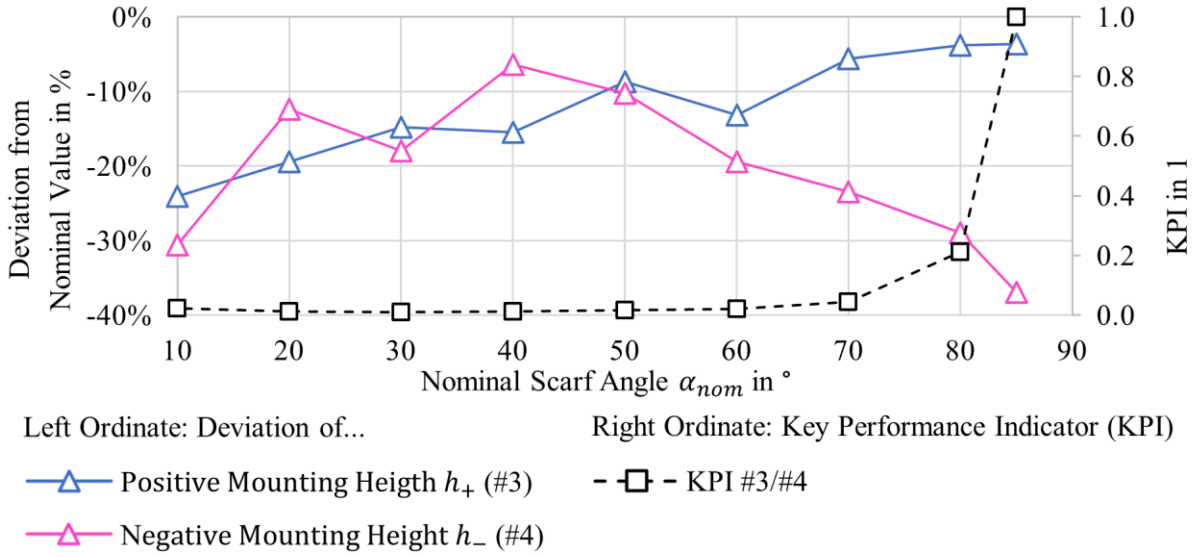

Figure 4. Deviation of the actual mounting height h from the respective nominal values and normalized KPI derived from optical measurement of positive (#3) and negative (#4) pyramids with varying nominal scarf angles α_{nom}

The actual base triangle side lengths of the pyramids examined on sample #3/#4 are not shown in Figure 4 as the deviation from the nominal value $a_{nom} = 1.5$ mm is not a function of the nominal scarf angle α_{nom}. The behavior corresponds to that already observed with sample #1/#2 (see Figure 3, pyramid with $a_{nom} = 1.5$ mm and $\alpha_{nom} = 60°$). The positive pyramids actual side lengths exceed the corresponding nominal value by approximately 5%, while the negative pyramids actual side lengths stay below the nominal value by 5%, regardless of the nominal scarf angle.
The actual mounting height of the pyramids on sample #3/#4 behaves quantitatively as in the samples with variable side lengths (#1/#2). All actual values stay below their respective nominal values, with the deviation of positive pyramids decreasing for larger nominal scarf angles and the deviation of negative pyramids increasing for larger nominal scarf angles. To improve the accuracy of fit, a reduced nominal mounting height $h_{nom,inc2}$ for negative pyramids according to equation 8 can be used.

$$h_{nom,inc2} = h_{nom} * \left(1 + f_{comp,h2}\right) \tag{8}$$

$$\text{using } f_{comp,h2} = \left(0.00010 * \frac{h_{nom}{}^2}{\text{mm}^2} - 0.0095 * \frac{h_{nom}}{mm} + 0.12\right)$$

$$\text{for } 10° \leq \alpha_{nom} \leq 85° \text{ and } a_{nom} = 1.5 \text{ mm}$$

Although the loss in mounting height is very high for negative pyramids, the advantage of an increased scarf angle outweighs the loss in actual adhesive surface area A_{Adh} considering the course of the KPI as a function of the scarf angle. This means that in order to implement 3D µSAJ using PBF-LB/M/AlSi10Mg triangular pyramids, the largest possible nominal scarf angle should be aimed for.

3.2. Static tensile tests

The results of the static tensile tests regarding the bonding strength of ABJs, 1D and 3D µSAJs are depicted in Figure 5.

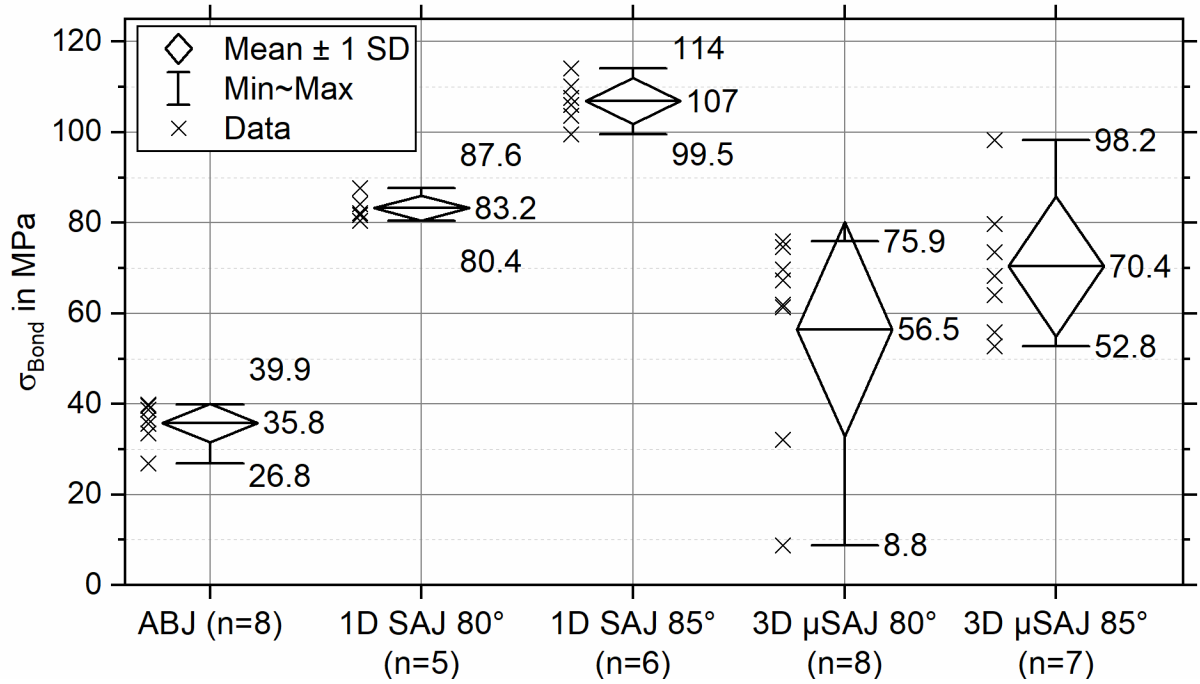

Figure 5. Bonding strength σ_{Bond} (according to equation 1) of adhesive butt joints (ABJs), 1D scarf adhesive joints (1D SAJs, $\alpha_{nom} = 80°/\alpha_{nom} = 85°$) and 3D micro scarf adhesive joints (3D µSAJs, $\alpha_{nom} = 80°/\alpha_{nom} = 85°$) resulting from static tensile tests

To determine the statistical significance of the difference in bonding strength, a two-tailed homoscedastic T-Test with a significance level of $\beta = 5\%$ was executed. The Shapiro-Wilk test was carried out to check whether the data in the samples follow a normal distribution and the Levene test was conducted to check homoscedasticity. These tests were passed by all samples, which confirms the applicability of the T-Test. The corresponding P-Values are documented in Table 4. (Lovric, 2011)

Table 4. P-Values (and Power) of two-tailed homoscedastic T-Test (significance level of β=0.05) to verify the statistical significance of the difference in bonding strength of different adhesive joint types

Type	(A) 1D SAJ 85°	(B) 1D SAJ 80°	(C) 3D µSAJ 85°	(D) 3D µSAJ 80°
(1) 1D SAJ 80°	3.34E-06 (1.00)	-	-	-
(2) 3D µSAJ 85°	9.37E-05 (0.99)	5.02E-02 (0.28)	-	-
(3) 3D µSAJ 80°	1.36E-04 (0.97)	1.54E-02 (0.49)	1.04E-01 (0.20)	-
(4) ABJ	1.04E-12 (1.00)	9.74E-11 (1.00)	1.90E-05 (0.99)	1.45E-02 (0.41)

As the condition of $\beta > P$ is met by all the pairs of varieties except for (2)/(B) and (3)/(C) it is verified that for the remaining combinations a difference in bonding strength exists. For the pairs of varieties not meeting the condition of $Power > 0.8$ ((2)/(B); (3)/(B); (3)/(C)) and (4)/(D)), the statistical significance of this difference in bonding strength is questionable and must be substantiated by additional tests to increase the sample size.

The mean value of the bonding strength of 1D SAJs using a nominal scarf angle of 85° exceeds the bonding strength of ABJs by 300% and the bonding strength of 3D µSAJs (with identical scarf angle) by 53%. This can be explained by the fact that manufacturing inaccuracies regarding the actual base triangle side length and mounting height of 3D µSAJs were not compensated in the tensile samples and therefore exhibit a negative effect on the accuracy of fit and thus also on the bonding strength. In addition, depending on the actual adhesive fill gap thickness, the plane-parallel portion of the negative and positive pyramid´s opposing adhesive surfaces is reduced to a larger extent in 3D µSAJs compared to 1D SAJs which possibly exhibits further negative influence on the bonding strength.
The positive effect of an increased scarf angle on the bonding strength is reflected in the results for 1D SAJs (increased by 29%) and 3D µSAJs (increased by 25%) to almost the same extent. The wide scatter in bonding strength among 3D µSAJs, as compared to ABJs and 1D SAJs, can be ascribed to challenges in achieving a homogenous adhesive layer, which is due to manufacturing variations among individual pyramids (which were not yet taken into account in the optical measurements).
If the joint´s performance is evaluated by relating the bonding strength to the nominal mounting height, the advantage of the 3D µSAJ becomes clear. By exhibiting a bonding strength to mounting height ratio of 1.8 kN/mm ($\alpha_{nom} = 80°$) respectively 1.1 kN/mm ($\alpha_{nom} = 85°$) the performance of the 3D µSAJ exceeds the performance of the 1D SAJ joint exhibiting an equivalent ratio of 0.11 kN/mm ($\alpha_{nom} = 80°$) respectively 0.073 kN/mm ($\alpha_{nom} = 85°$) by a factor of 15.

4. Conclusion and outlook

This study has shown the feasibility of tapering a scarf adhesive joint in multiple planes by applying positive triangular pyramids and imprinting corresponding negative triangular pyramids to the front surfaces of PBF-LB/M/AlSi10Mg substrates.
Optical measurement of PBF-LB/M/AlSi10Mg pyramid geometry samples revealed an ideal base triangle side length for the triangular pyramids of $a_{nom} = 1.5$ mm and that the shaft angle α_{nom} should be chosen as large as possible (examined up to 85°) to maximize the joints performance. To improve the accuracy of fit and to compensate for manufacturing inaccuracies between positive and negative pyramids, the nominal base triangle side length of positive pyramids and the nominal mounting height of negative pyramids can be modified according to the compensation functions specified in equation 6; 7 and 8. The impact of applying the compensation functions to the respective nominal values on the accuracy of fit will be evaluated by optical measurement of corresponding pyramid geometry samples in the near future. To capture manufacturing variations between individual pyramids, several identical pyramid geometry samples will be examined as part of these investigations.
Static tensile tests showed that the bonding strength to mounting height ratio of 3D µSAJs exceeds the equivalent ratio of 1D SAJs by a factor of 15, even without compensating for manufacturing inaccuracies. Since part separation and subsequent adhesive bonding of AM sub-parts implies maximum bonding strength at a minimum use of substrate volume, 3D µSAJs can contribute to this design approach for additive manufacturing. Further investigation must cover the effects of an improved accuracy of fit and the influence of the actual adhesive fill gap thickness on the bonding strength. Apart from pure tensile loading, static and fatigue tests will cover additional load cases like bending, torsion and their superimposition.
Since other additive manufacturing processes also exhibit limitations regarding the maximum part complexity and size, future studies should concern the feasibility and effectiveness of 3D µSAJs using alternative additive manufacturing processes (e.g. PBF-LB/P; DED; MEX or MJT) and materials (e.g. Ti6Al4V; PA12; ABS or TPU). This way, the advantages of part separation and subsequent joining of AM sub-parts as a self-contained design approach for additive manufacturing can be further exploited and successfully implemented in academic and industrial applications.

Acknowledgement

This research is part of the project FLAB-3Dprint and funded by dtec.bw – Digitalization and Technology Research Center of the Bundeswehr, which we gratefully acknowledge. dtec.bw is funded by the European Union – NextGenerationEU.

References

Banea, M.D. and Da Silva, L.F.M. (2009), "Adhesively bonded joints in composite materials: An overview", *Proceedings of the Institution of Mechanical Engineers*, Vol. 223 No. 1, pp. 1–18. https://doi.org/10.1243/14644207JMDA219

Diegel, O., Nordin, A. and Motte, D. (2019), A Practical Guide to Design for Additive Manufacturing, Springer Singapore, Singapore. https://doi.org/10.1007/978-981-13-8281-9

Ebnesajjad, S. and Landrock, A.H. (2015), Adhesives Technology Handbook, 3. ed., Elsevier, Amsterdam. https://doi.org/10.1016/C2013-0-18392-4

EN (2009), EN 15870:2009: Adhesives – Determination of tensile strength of butt joints, European Committee for Standardization, Berlin.

Gacoin, A., Lestriez, P., Assih, J., Objois, A. and Delmas, Y. (2009), "Comparison between experimental and numerical study of the adhesively bonded scarf joint and double scarf joint: Influence of internal singularity created by geometry of the double scarf joint on the damage evolution", *International Journal of Adhesion and Adhesives*, Vol. 29 No. 5, pp. 572–579. https://doi.org/10.1016/j.ijadhadh.2009.01.006

Lovric, M. (2011), International encyclopedia of statistical science, *Springer reference*, Springer, Berlin. https://doi.org/10.1007/978-3-642-04898-2

Panesar, A., Abdi, M., Hickman, D. and Ashcroft, I. (2018), "Strategies for functionally graded lattice structures derived using topology optimisation for Additive Manufacturing", *Additive Manufacturing*, Vol. 19, pp. 81–94. https://doi.org/10.1016/j.addma.2017.11.008

Reichwein, J., Geis, J., Rudolph, K. and Kirchner, E. (2022), "Design guidelines for the separation of components to combine the potentials of additive and conventional manufacturing processes", *Procedia CIRP*, Vol. 109, pp. 592–597. https://doi.org/10.1016/j.procir.2022.05.319

Reichwein, J. and Kirchner, E. (2021), "Part orientation and separation to reduce process costs in additive manufacturing", *Proceedings of the Design Society*, Vol. 1, pp. 2399–2408. https://doi.org/10.1017/pds.2021.501

Yang, L., Hsu, K., Baughman, B., Godfrey, D., Medina, F., Menon, M. and Wiener, S. (2017), Additive Manufacturing of Metals: The Technology, Materials, Design and Production, Springer International Publishing, Cham. https://doi.org/10.1007/978-3-319-55128-9

Yang, S. and Zhao, Y.F. (2015), "Additive manufacturing-enabled design theory and methodology: a critical review", *The International Journal of Advanced Manufacturing Technology*, Vol. 80 No. 1-4, pp. 327–342. https://doi.org/10.1007/s00170-015-6994-5